Improved Rear Surface Passivation of Cu(In,Ga)Se_2 Solar Cells: A Combination of an Al_2O_3 Rear Surface Passivation Layer and Nanosized Local Rear Point Contacts

Bart Vermang, Viktor Fjällström, Xindong Gao, and Marika Edoff

***Abstract*—An innovative rear contacting structure for copper indium gallium (di) selenide (CIGS) thin-film solar cells is developed in an industrially viable way and demonstrated in tangible devices. The idea stems from the silicon (Si) industry, where rear surface passivation layers are combined with micron-sized local point contacts to boost the open-circuit voltage (V_{OC}) and, hence, cell efficiency. However, compared with Si solar cells, CIGS solar cell minority carrier diffusion lengths are several orders lower in magnitude. Therefore, the proposed CIGS cell design reduces rear surface recombination by combining a rear surface passivation layer and nanosized local point contacts. Atomic layer deposition of Al_2O_3 is used to passivate the CIGS surface and the formation of nanosphere-shaped precipitates in chemical bath deposition of CdS to generate nanosized point contact openings. The manufactured Al_2O_3 rear surface passivated CIGS solar cells with nanosized local rear point contacts show a significant improvement in V_{OC} compared with unpassivated reference cells.**

***Index Terms*—Al_2O_3, atomic layer deposition, copper indium gallium selenide (CIGS), Cu(In,Ga)Se_2, Ga grading, nanosized, passivated emitter, passivated emitter and rear cell (PERC), photovoltaics, point contact openings rear locally diffused cell (PERL), rear surface passivation, Si, solar cells, thin film.**

I. Introduction

At present, rear surface recombination in highly efficient copper indium gallium (di)selenide (CIGS) solar cells is limited by using Ga grading to create a back surface field (BSF). World record conversion efficiencies (Eff.) of lab-scale CIGS solar cells are around 20%. Some recent outstanding examples are 1) the Japanese thin film manufacturer Solar Frontier, claiming a cadmium-free CIGS solar cell efficiency record of 19.7%, and 2) the Swiss Federal Laboratories for Materials Science and Technology (EMPA), who have announced a thin-film CIGS solar cell record of 20.4% on a flexible polymer substrate [1]–[5]. These high efficiencies are achieved by varying the [Ga]/([Ga]+[In]) ratio to obtain different band gaps at different depths in the CIGS film. To reduce rear surface recombination, an increase of this ratio and, thus, bandgap toward the Mo back contact is a standard practice [6]. See, e.g., Fig. 1, which shows a scanning electron microscopy (SEM) cross section of a Mo/CIGS structure (produced adjacent to a 20.0% CIGS solar cell) fabricated by increasing the [Ga]/([Ga]+[In]) ratio toward the Mo/CIGS rear interface [4]. This gradient causes a quasi-electrical BSF that keeps the minority charge carriers away from the Mo/CIGS interface, and effectively reduces rear surface recombination [6].

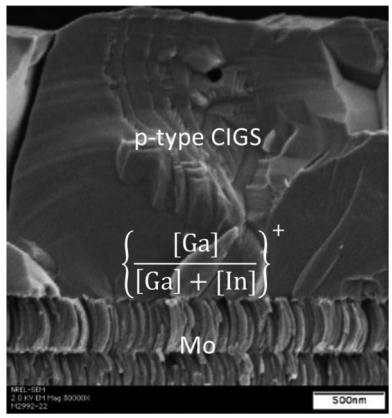

Fig. 1. SEM cross-section picture of a Mo/CIGS structure with a cell efficiency potential of 20.0% (taken from [4]).

In Si solar cell manufacturing, the present-day workhorse is the full aluminum (Al) BSF p-type silicon (Si) solar cell, whose rear structure is very comparable with those high-efficient CIGS cells. Fig. 2(a) represents a sketch of such a traditional full Al BSF cell. At the rear Al/Si interface, a BSF is formed thanks to a highly Al-doped p^+ region. In addition, in this case, the purpose of this BSF is to keep photo-electrons away from the metal/semiconductor (Al/Si) interface and, as a result, to reduce rear surface recombination [7].

Nevertheless, more advanced passivated emitter and rear cell (PERC) and analogous cell designs are on their way to substitute conventional aluminum Al BSF Si solar cells [8]–[10]. Fig. 2(b) represents a sketch of this alternative PERC [7]. As can be seen,

Manuscript received June 10, 2013; revised August 29, 2013; accepted October 15, 2013. Date of publication November 12, 2013; date of current version December 16, 2013. This work was supported by the Swedish Science Foundation (VR) and the Swedish Energy Agency. The work of B. Vermang was supported by the European Commission via FP7 Marie Curie IEF 2011 Action No. 300998.

B. Vermang, V. Fjällström, and M. Edoff are with the Ångström Solar Center, Division of Solid State Electronics, Department of Engineering Sciences, Uppsala University, 75121 Uppsala, Sweden (e-mail: Bart.Vermang@angstrom.uu.se; Viktor.Fjallstrom@angstrom.uu.se; Marika.Edoff@angstrom.uu.se).

X. Gao is with the Division of Solid State Electronics, Department of Engineering Sciences, Uppsala University, 75121 Uppsala, Sweden (e-mail: Gao.Xindong@angstrom.uu.se).

Color versions of one or more of the figures in this paper are available online at http://ieeexplore.ieee.org.

Digital Object Identifier 10.1109/JPHOTOV.2013.2287769

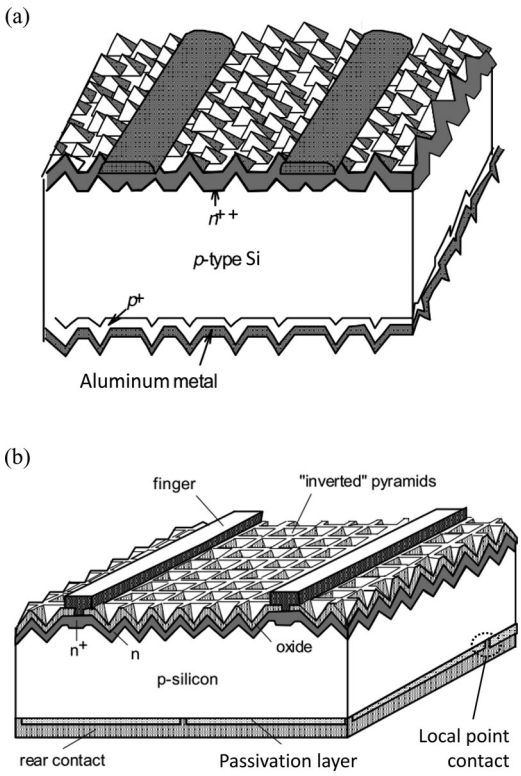

Fig. 2. Schematic drawing of (a) the conventional full Al back surface field p-type Si solar cell and (b) the passivated emitter and rear p-type Si solar cell (taken from [7]).

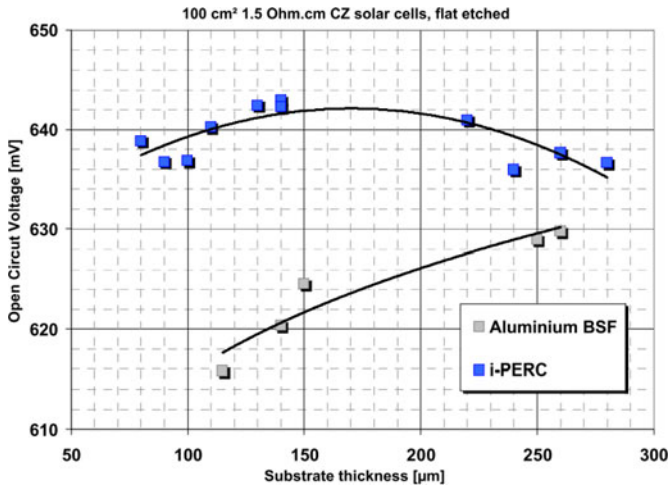

Fig. 3. Comparison of open-circuit voltages as a function of Si substrate thickness for (■) rear surface passivated industrial PERC (i-PERC) cells and (▒) standard full Al BSF reference cells (taken from [20]).

with respect to a conventional Al BSF solar cell production line, only a few extra steps are needed to introduce PERC processing: single-side texturing, local diffusion technologies, passivation layer deposition, and passivation layer opening. The potential of this more advanced cell processing is exposed by referring to the 25% world record cell conversion efficiency for single-junction Si solar cells as this record is achieved applying the passivated emitter, rear locally diffused cell (PERL) design, which is a PERC combined with locally diffused rear point contacts [1], [11].

Compared with conventional Al BSF processing, the rear of those advanced Si cell designs (PERC/PERL) is improved by a combination of an adequate rear surface passivation layer and micron-sized local point contacts—as shown in Fig. 2(b). Such a passivition layer combines two passivation mechanisms: 1) chemical passivation—a low density of interface defects D_{it} and 2) field-effect passivation—caused by a high density of fixed charges within the passivation layer. Roughly said, the point contact opening diameter has to be on the order of 50 to 200 μm, with a distance of 400 to 1600 μm between contact openings, as the minority carrier diffusion length L_n in industrial p-type Si wafers is in the order of 200 to 800 μm—depending on Si material quality and the doping level [8]–[10], [12]. Characteristic surface passivation layers for p-type Si are a combination of aluminum oxide (Al_2O_3), silicon oxide (SiO_2), and hydrogenated silicon nitride (SiN_x:H) [13], [14], while the local point contacts are generated industrially by applying laser technology and represent 2 to 5% of the total rear surface area [8]–[10], [15]–[17].

Those rear surface passivation technologies are cost-effective for Si solar industry. They increase cell efficiency and allow the use of ever thinner wafers (resulting in a reduction in material cost), by improvements in rear surface passivation and rear internal reflection. In the case of standard full Al BSF solar cells, the rear surface recombination velocity S_b and rear internal reflection R_b generally are in the order of 1×10^4 to 1×10^6 cm/s and 60 to 70%, respectively. Unfortunately, this means that for full Al BSF cells a reduction in wafer thickness will decrease cell efficiency, because of 1) a raise in surface recombination—due to an increased surface-to-volume ratio combined with insufficient surface passivation and 2) a loss in absorption—due to thinner cells combined with low rear internal reflection. Rear surface passivated cell designs, on the other hand, lead to S_b as low as 1×10^2 cm/s and R_b above 85% and, hence, enhanced cell efficiencies for thinner Si wafers [8], [14], [18], [19]. Typically, short-circuit current J_{SC} is increased slightly due to higher R_b, while the fill factor FF is reduced somewhat due to more challenging contacting schemes. Nevertheless, due to an absolute improvement in rear surface passivation the open-circuit voltage V_{OC} is enhanced significantly. See, for example, Fig. 3, which compares V_{OC} of rear surface passivated i-PERC Si solar cells with standard full Al BSF cells as a function of Si wafer thickness [20]. Practically speaking, 300-μm-thick standard Al BSF Si solar cells can be substituted by more efficient rear surface passivated cells with a thickness between 100 and 200 μm.

Therefore, the purpose of this study is to assess the potential of these rear surface passivation technologies in CIGS solar cells. As for Al BSF Si cells, the Mo/CIGS rear surface of normal Ga-graded CIGS cells is known to show high S_b (also between 1×10^4 and 1×10^6 cm/s [21]–[23]) and low R_b (see the next section for R_b as a function of wavelength for the Mo/CIGS interface). Hence, analogous to Si PERC, the proposed cell design combines a rear surface passivation layer and local rear point contacts (LRPC), enabling reduced back contact

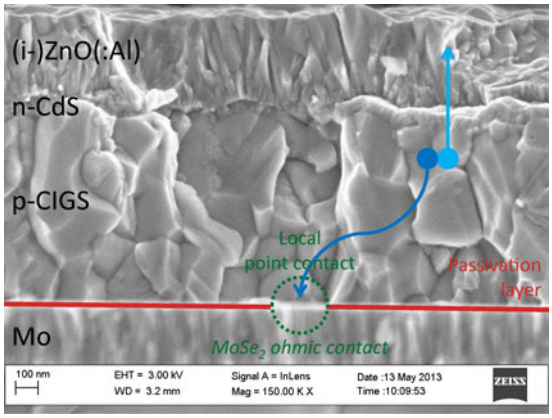

Fig. 4. Proposed CIGS solar cell design to reduce back contact recombination, by combining a rear surface passivation layer and local rear point contacts.

recombination and, thus, higher efficiencies—particularly for ever thinner CIGS absorber layers. However, thin film solar cells are known to have very short minority carrier lifetimes, which means that LRPC for rear passivated CIGS cells require to be nanosized and closely spaced. Assuming that L_n between 0.75 and 1.50 μm is feasible [24], [25], the contact openings targeted are between 200 and 400 nm in diameter with internal spacing between 1.5 and 3.0 μm, as scaled from the Si PERC design and keeping the contacting area between 2 and 5% of the total rear surface area. Fig. 4 shows a graphical representation of this proposed cell design.

This novel rear contacting structure for CIGS solar cells is developed in an industrially viable way and its improvement—compared with state-of-the-art reference cells—is demonstrated in tangible devices as a function of CIGS absorber layer thickness.

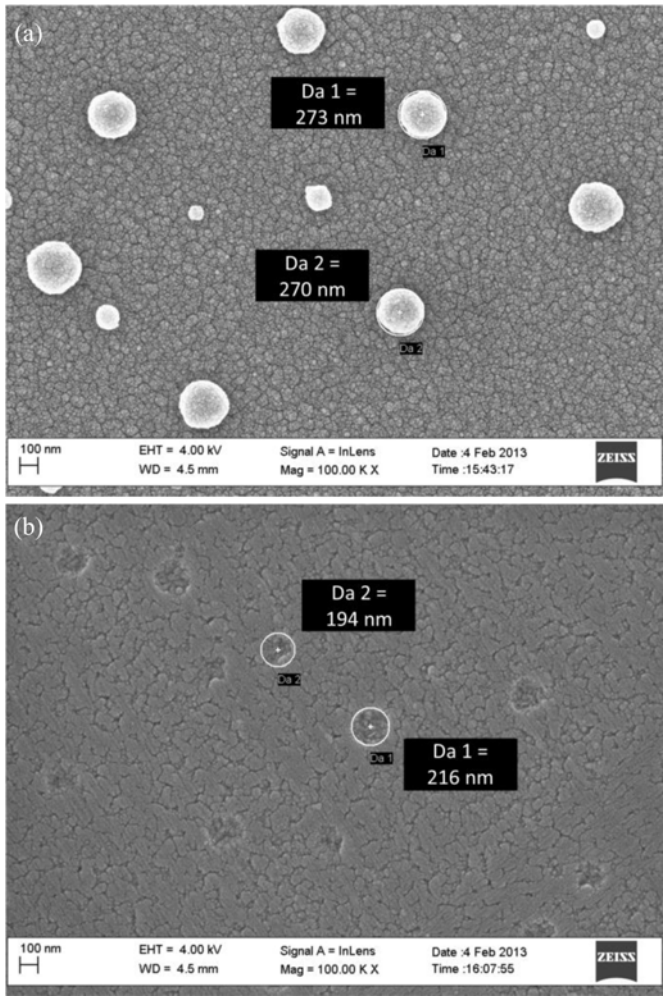

Fig. 5. SEM pictures of (a) a particle-rich CdS layer grown on a SLG/Mo substrate and (b) the same substrate after CdS particle removal (taken from [27]).

II. Methodology

The formation and subsequent removal of spherical particles (so-called colloids or precipitates) in chemical bath deposition (CBD) of CdS is applied to generate nanosized point contacts. In this study, standard CBD CdS is grown in a solution with 1.136 M ammonia, 0.100 M thiourea, and 0.003 M cadmium acetate, at 60 °C. However, to obtain particle-rich CdS deposition conditions, an alternative approach is required: 1) After preparing the CBD solution, soda lime glass (SLG)/Mo substrates are only immersed when the CBD solution reacted for X min—during which time CdS nanoparticles are formed within the solution [26]. 2) Thereafter, the substrates are dipped for Y min, and a thin particle-rich CdS film is grown. By varying time intervals X and Y the particle-density can be varied. Fig. 5 shows top-view SEM pictures of thin particle-rich CdS layers deposited on SLG/Mo substrates before and after removal of these particles [27]; in this case, both X and Y equal 4 min, and an extra layer of CdS is grown to intensify the contrast in Fig. 5(b). Particle removal is established in various ways: via 1) ultrasonic agitation, 2) dry ice (liquid CO_2) cleaning, or 3) mechanical wiping. Using numerous SEM measurements, an average particle diameter of 285 $\pm$ 30 nm and average point opening diameter of 220 $\pm$ 25 nm is calculated. In conclusion, to actually create nanosized point openings in rear surface passivation layers for CIGS, the passivation layer is 1) first grown on this particle-rich CdS layer, and 2) subsequently, the particles are removed. This way, a passivation layer with nanosized point openings having a diameter around 220 nm is obtained.

Atomic layer deposition (ALD) of Al_2O_3 is applied as CIGS surface passivation layer. In this study, ALD Al_2O_3 passivation layers are deposited in a temporal ALD reactor at 300 °C, using trimethylaluminum (TMA) and an oxygen source (both water (H_2O) and ozone (O_3) are used) as precursors [28]. Previously, Al_2O_3 is verified to be an adequate CIGS surface passivation layer, thanks to its 1) chemical passivation—first principles calculations indicate that the deposition of Al_2O_3 reduces about 35% of the interface defect density—and 2) field effect passivation—Al_2O_3 exhibits a large density of negative charges, causing a field effect that reduces the CIGS surface minority charge carrier concentration and, hence, passivates the interface effectively [23]. In the same work, an improvement of two orders in magnitude is reported for the integrated photoluminescence intensity of Al_2O_3 passivated CIGS compared

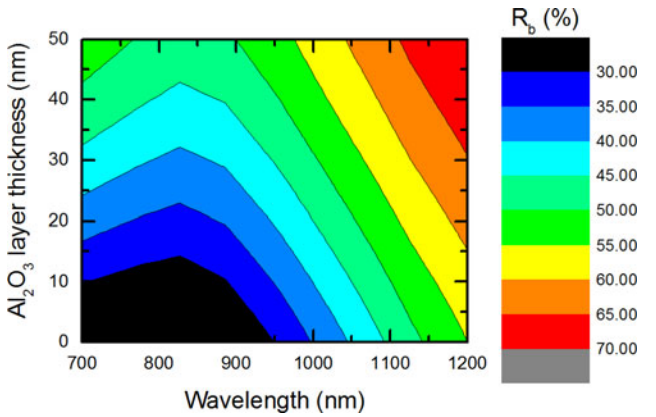

Fig. 6. Calculated rear internal reflection as a function of wavelength and Al_2O_3 layer thickness for a Mo/(CdS/)Al_2O_3/CIGS device [29].

with unpassivated CIGS. Hence, a significant reduction in S_b is expected for Al_2O_3 passivated CIGS surfaces compared with standard Mo/CIGS surfaces. To also have an idea about its optical confinement, R_b at the Mo/(CdS/)Al_2O_3/CIGS interface is calculated as in [29]; applying thickness, refractive index and extinction coefficient of the Al_2O_3 layer as measured on an Si substrate using spectrally resolved ellipsometry. In Fig. 6, R_b is depicted as a function of long wavelength and Al_2O_3 layer thickness in the case of a Mo/(CdS/)Al_2O_3/CIGS structure. This shows that—compared with the standard Mo/CIGS interface (equivalent to an Al_2O_3 layer thickness of 0 nm)—applying a thin layer (e.g., 5 nm) of Al_2O_3 as rear surface passivation increases R_b only slightly, while a thicker Al_2O_3 layer (e.g., 50 nm) leads to a larger R_b enhancement.

Ungraded CIGS absorber layers are used [30] 1) to allow evaluation of an obvious improvement in V_{OC} if rear surface passivation is enhanced and 2) to exclude any other surface passivation effects. CIGS layers are deposited in a high-vacuum chamber equipped with open-boat evaporation sources, while evaporation rates are monitored using a mass spectrometer. During CIGS growth, the maximum substrate temperature is 540 °C; Se is evaporated in excess; and constant rates of Cu, In, and Ga are applied until a desired CIGS thickness is reached. All studied samples have compositional values of [Cu]/([Ga] + [In]) = 0.90 ± 0.02 and [Ga]/([Ga] + [In]) = 0.30 ± 0.01, which are calculated from X-ray fluorescence (XRF) measurements. CIGS film thicknesses are measured with a profilometer and are varied between 0.48 ± 0.02 and 1.58 ± 0.04 μm. These "flat-evaporation-rate-CIGS" absorbers with uniform low Ga concentration are favored to assess rear surface passivation, because of their high reproducibility, their characteristic high L_n [24], and to exclude complementary rear surface passivation effects (e.g., a quasi-electrical field created by a Ga gradient causing a slope in the conduction band—as is the case in standard high-efficient CIGS cells). This approach leads to cell efficiencies below 16.5%, but allows an evident boost in solar cell characterization results if the advanced CIGS cell design functions.

Table I gives an overview of all steps required to fabricate rear surface passivated CIGS solar cells with nanosized LRPC. A detailed description of standard CIGS solar cell processing at the Ångström Solar Center can be found in [31], i.e., excluding

TABLE I
OVERVIEW OF ALL STEPS REQUIRED TO FABRICATE AL_2O_3 REAR SURFACE PASSIVATED CIGS SOLAR CELLS WITH NANO-SIZED LOCAL REAR POINT CONTACTS

Step	Description
0	Start: low-iron soda lime glass
1	Glass cleaning
2	Mo rear contact sputtering
3	Particle-rich CBD CdS deposition
4	ALD Al_2O_3 passivation deposition
5	CdS particle removal
6	Ungraded CIGS absorber co-evaporation
7	CBD CdS buffer deposition
8	(i-)ZnO(:Al) window sputtering
9	Ni/Al/Ni front contact evaporation
10	Mechanical scribing of 0.5 cm^2 solar cells

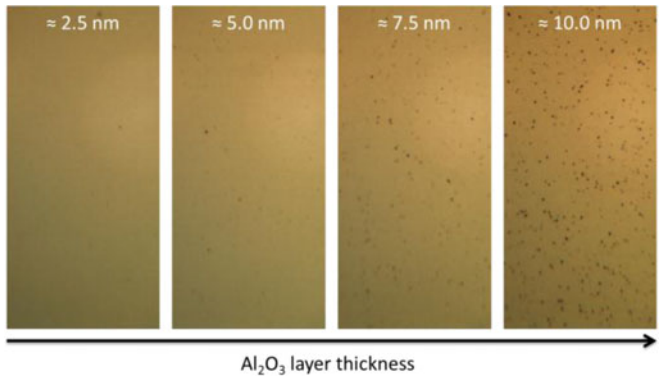

Fig. 7. Top-view optical microscopy pictures after particle removal of SLG/Mo/particle-rich-CdS/Al_2O_3 samples as a function Al_2O_3 layer thickness.

the ungraded absorber layer formation and the advanced back contact design. The starting substrate is low-iron SLG with a thickness of 1 mm, which first undergoes a cleaning process. As back contact, a Mo layer is deposited in an inline sputtering system. It has a sheet resistance of 0.6 Ω/□ and a typical thickness of 350 nm. The advanced back contact design combines an ALD Al_2O_3 rear surface passivation layer and CBD of CdS to generate nanosized LRPC, as described previously. On top of this rear contact structure, an ungraded CIGS absorber layer of desired thickness is evaporated, alsodescribed previously. The buffer layer is deposited using a standard CBD CdS process. Next, the shunt reducing intrinsic ZnO layer (i-ZnO) and, subsequently, the Al-doped ZnO (ZnO:Al) front contact of the cells are sputtered. As front contact grid, a Ni/Al/Ni stack is deposited by evaporation through a shadow mask. The (i-)ZnO(:Al) and Ni/Al/Ni stack have a total thickness around 400 and 3000 nm, respectively. Finally 0.5 cm^2 solar cells are defined by mechanical scribing with a stylus. No antireflective coating is used.

Light *J–V* measurements are performed at 25 °C under standard AM1.5 G conditions in a home-made system with a tungsten halogen lamp, which is calibrated using a certified silicon photo diode [31].

III. RESULTS AND DISCUSSION

The proposed technique to create nanosized point openings in Al_2O_3 passivation layers—by removing spherical particles deposited by CBD CdS—works fine for Al_2O_3 layers that are not too thick (≤5 nm). Fig. 7 depicts for various Al_2O_3 thicknesses and top-view optical microscopy pictures of SLG/Mo/

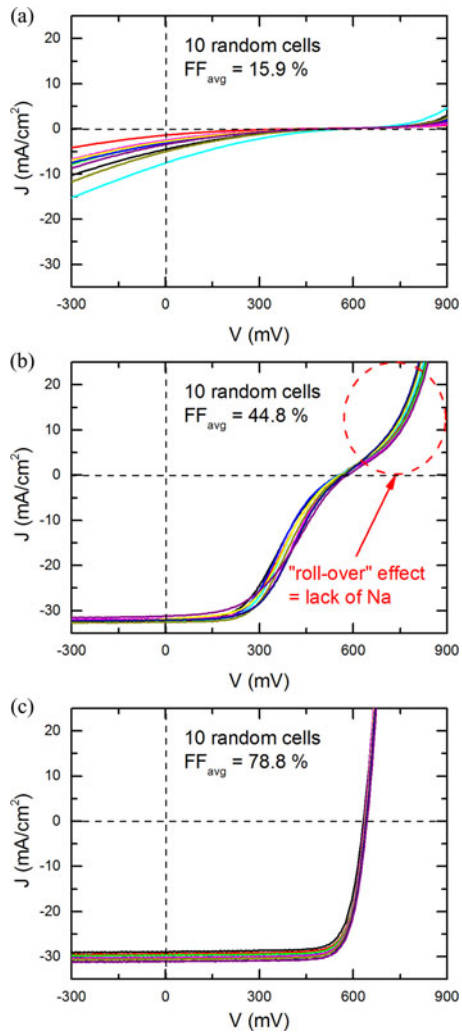

Fig. 8. Representative *J–V* curves for (a) Al_2O_3 rear surface passivated CIGS solar cells without nanosized LRPC, (b) Al_2O_3 rear surface passivated CIGS cells with nanosized LRPC, and (c) Al_2O_3 rear surface passivated CIGS cells having nanosized LRPC and an additional NaF layer evaporated on top of the Al_2O_3 layer (after particle removal). In all examples, the Al_2O_3 and CIGS layer thickness are around 5.0 nm and 1.58 μm, respectively. In each case, 10 random *J–V* curves are shown, and the average fill factor is given.

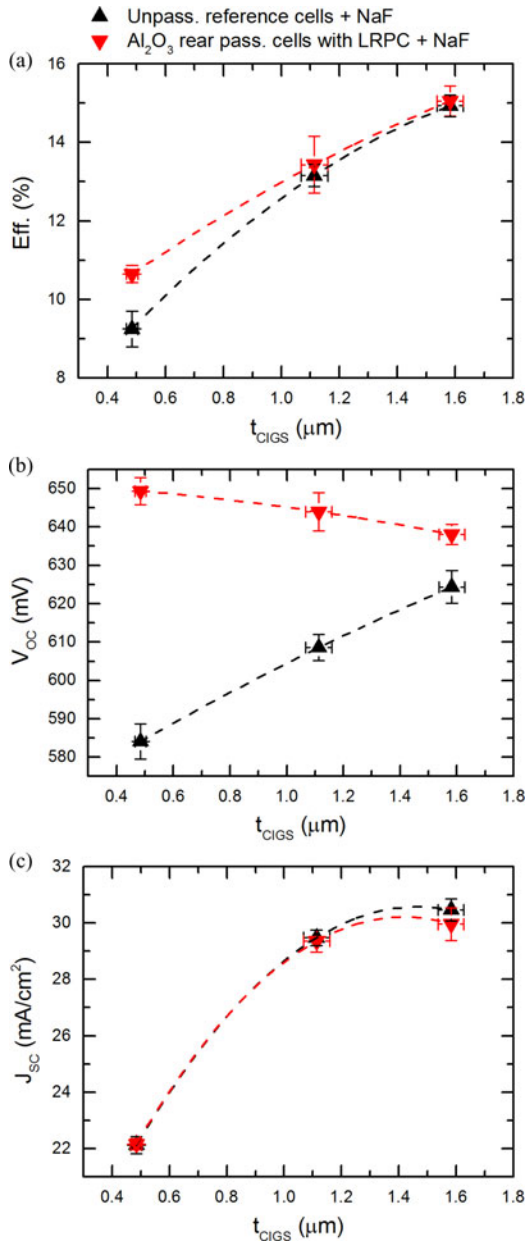

Fig. 9. Average (a) cell conversion efficiency, (b) open-circuit voltage, and (c) short-circuit current as a function of CIGS absorber layer thickness for Al_2O_3 rear surface passivated CIGS solar cells having nanosized LRPC compared with unpassivated reference CIGS cells. For each CIGS thickness, the same optimized NaF thickness is used for both the passivated and the unpassivated cells. Standard deviation is shown as error bars.

particle-rich-CdS/Al_2O_3 structures after particle removal. These pictures show that for too-thick ALD Al_2O_3 films ($\geq$7.5 nm), the particle removal becomes unsatisfactory. The self-limiting nature of ALD reactions leads to an ideal growth control and the ability to coat high-aspect-ratio structures, as desired for the suggested point opening approach. However, these ALD advantages also mean that CdS nanoparticles embedded in too-thick Al_2O_3 films become irremovable. Therefore, 5 nm of Al_2O_3 has been used for all passivated cells with LRPC, which are described next.

Al_2O_3 rear surface passivated CIGS solar cells require 1) LRPC for appropriate contacting and 2) extra supply of Na—since Al_2O_3 layers act as a barrier for Na diffusion from the SLG substrate. Fig. 8(a) shows representative *J–V* curves for ten random Al_2O_3 rear surface passivated CIGS solar cells without LRPC. These cells have an average FF of 16%, which 1) proves that there is no appropriate back contacting without point contacts and 2) indicates that the passivation layer is intact after CIGS processing. Fig. 8(b), on the other hand, shows representative *J–V* curves for 10 random Al_2O_3 rear surface passivated CIGS cells with nanosized LRPC. The average FF increases to 45%, higher compared with the cells without LRPC but still rather low. In addition, these *J–V* curves show a "roll-over" effect, characteristic for devices lacking Na [32]. Note that 1) Al_2O_3 films are known to be excellent gas diffusion barriers [33] and that 2) this roll-over effect is not as pronounced as in Na-free cells [32]. Therefore, Fig. 8(c) shows representative *J–V* curves for 10 random Al_2O_3 rear surface passivated CIGS cells having LRPC and—after removal of the

CdS nanoparticles—an additional NaF layer evaporated on top of this Al_2O_3 layer. Fig. 8(c) proves that the low FF's in Fig. 8(b) are indeed caused by Al_2O_3 acting as an Na diffusion barrier. Even more, the combination of LRPC and extra Na supply leads to a high average FF of 79%.

The rear surface of Al_2O_3 rear surface passivated CIGS solar cells with nanosized LRPC are better passivated compared with unpassivated reference cells, which becomes more obvious in the case of thinner CIGS absorber layers. Fig. 9 shows the average 1) Eff., (b) V_{OC}, and (c) J_{SC} as a function of CIGS absorber layer thickness for Al_2O_3 rear surface passivated CIGS solar cells having nanosized LRPC and unpassivated reference CIGS cells. Note that for each CIGS thickness, the same optimized NaF thickness is used for both the Al_2O_3 passivated and the unpassivated reference cells. Fig. 9(a) shows that higher average efficiencies are measured for all the Al_2O_3 rear passivated cells. In addition, the difference becomes more apparent for the thinnest CIGS layers. Fig. 9(b) demonstrates that this increase in efficiency is obtained thanks to an improvement in V_{OC} for the Al_2O_3 rear passivated cells. The most logical explanation for this increase in V_{OC} is a significant enhancement in rear surface passivation (=lower S_b) for the Al_2O_3 rear-passivated cells [23], [27]. This boost in surface passivation becomes clearer for thinner CIGS absorber layers, as this well-passivated rear surface then gets closer to the space charge region of the cell. In addition, it is remarkable that this change in V_{OC} as a function of absorber layer thickness for rear passivated compared with unpassivated cells is very similar to Fig. 3. Unfortunately, the average J_{SC} of the passivated and unpassivated cells is similar for all CIGS thicknesses, as seen in Fig. 9(c). This comparable behavior in J_{SC} for passivated and unpassivated cells can be explained by a too-small improvement in R_b for only 5 nm of Al_2O_3 as rear surface passivation layer, as already shown in Fig. 6.

IV. Conclusion and Outlook

For the first time, the concept of rear surface passivation—as used in advanced Si cell technologies (PERC/PERL)—is developed for and shown in industrially viable CIGS solar cells: 5 nm of ALD Al_2O_3 is used to passivate the CIGS rear surface and the formation of nanosphere-shaped precipitates in CBD CdS to generate point contact openings. The same (V_{OC}) behavior is shown for rear surface passivated CIGS solar cells compared with unpassivated reference cells [see Fig. 9(b)] as for rear surface passivated Si solar cells compared unpassivated Si cells (see Fig. 3). Thanks to a significant improvement in rear surface passivation, an obvious increase in V_{OC} is measured, especially for ever thinner CIGS absorber layers, as this well-passivated rear surface gets closer to the most active region of the cells.

However, more reflective rear surface passivation layers need to be integrated to increase J_{SC} and, hence, efficiency, even further. As seen in Fig. 6, 5 nm of ALD Al_2O_3 increases R_b only slightly compared with the referential Mo/CIGS rear interface. Therefore, the focus is now on integrating thicker passivation layers to combine improved rear surface passivation with enhanced optical confinement. For that reason, research is ongoing to 1) combine Al_2O_3 rear surface passivation with other point contact opening approaches (lithography, laser ablation) or 2) combine the CBD CdS proposed technique to create nanosized point openings with other CIGS passivation layer candidates. The final target is—compared with unpassivated state-of-the-art CIGS solar cells of normal thickness—to develop CIGS cells having improved rear surface passivation and rear internal reflection, leading to a substantial increase in cell efficiency, even for thinner CIGS absorber layers.

References

[1] M. A. Green, "Solar cell efficiency tables (version 41)," *Prog. Photovoltaics, Res. Appl*., vol. 21, pp. 1–11, 2013.

[2] P. Reinhard, A. Chirila, P. Blosch, F. Pianezzi, S. Nishiwaki, S. Buecheler, and A. N. Tiwari, "Review of progress toward 20% efficiency flexible CIGS solar cells and manufacturing issues of solar modules," *IEEE J. Photovoltaics*, vol. 3, no. 1, pp. 572–580, Jan. 2013.

[3] P. Jackson, D. Hariskos, E. Lotter, S. Paetel, R. Wuerz, R. Menner, W. Wischmann, and M. Powalla, "New world record efficiency for Cu(In,Ga)Se_2 thin-film solar cells beyond 20%," *Prog. Photovoltaics, Res. Appl*., vol. 19, pp. 894–897, 2011.

[4] S. Niki, M. Contreras, I. Repins, M. Powalla, K. Kushiya, S. Ishizuka, and K. Matsubara, "CIGS absorbers and processes," *Prog. Photovolt, Res. Appl*., vol. 18, pp. 453–466, 2010.

[5] I. Repins, S. Glynn, J. Duenow, T. J. Coutts, W. Metzger, and M.A. Contreras, "Required material properties for high-efficiency CIGS modules," *Proc. SPIE*, vol. 7409, pp. 1–14, 2009.

[6] O. Lundberg, M. Edoff, and L. Stolt, "The effect of Ga-grading in CIGS thin film solar cells," *Thin Solid Films*, vol. 480–481, pp. 520–525, 2005.

[7] M.A. Green, "Crystalline silicon solar cells," in *Clean Electricity from Photovoltaics*. London, U.K.: Imperial College Press, 2001.

[8] Z. Wang, P. Han, H. Lu, H. Qian, L. Chen, Q. Meng, N. Tang, F. Gao, Y. Jiang, J. Wu, W. Wu, H. Zhu, J. Ji, Z. Shi, A. Sugianto, L. Mai, B. Hallam, and S. Wenham, "Advanced PERC and PERL production cells with 20.3% record efficiency for standard commercial p-type silicon wafers," *Prog. Photovoltaics, Res. Appl*, vol. 20, pp. 260–268, 2012.

[9] M. Moors, K. Baert, T. Caremans, F. Duerinckx, A. Cacciato, and J. Szlufcik, "Industrial PERL-type solar cells exceeding 19% with screen-printed contacts and homogeneous emitter," *Solar Energy Mater. Solar Cells*, vol. 106, pp. 84–88, 2012.

[10] A. Cacciato, F. Duerinckx, K. Baert, M. Moors, T. Caremans, G. Leys, M. Mrcarica, E. Picard, A. Ristow, and J. Szlufcik, "Industrial PERL-type Si solar cells with efficiencies exceeding 19.5%," *IEEE J. Photovoltaics*, vol. 3, no. 2, pp. 628–634, Apr. 2013.

[11] J. Zhao, A. Wang, and M.A. Green, "24% efficient PERL structure silicon solar cells," in *Proc. 21st IEEE Photovoltaic Spec. Conf*., 1990, pp. 333–335.

[12] J. A. Giesecke, M. Kasemann, and W. Warta, "Determination of local minority carrier diffusion lengths in crystalline silicon from luminescence images," *J. Appl. Phys*., vol. 106, pp. 014907-1–014907-8, 2009.

[13] B. Vermang, H. Goverde, L. Tous, A. Lorenz, P. Choulat, J. Horzel, J. John, J. Poortmans, and R. Mertens, "Approach for Al_2O_3 rear surface passivation of industrial p-type Si PERC above 19%," *Prog. Photovoltaics, Res. Appl*., vol. 20, pp. 269–273, 2012.

[14] T. Dullweber, S. Gatz, H. Hannebauer, T. Falcon, R. Hesse, J. Schmidt, and R. Brendel, "Towards 20% efficient large-area screen-printed rear-passivated silicon solar cells," *Prog. Photovoltaics, Res. Appl*., vol. 20, pp. 630–638, 2012.

[15] G. Agostinelli, J. Szlufcik, P. Choulat, and G. Beaucarne, "Local contact structures for industrial PERC-type solar cells," in *Proc. 20th Eur. Photovoltaic Sol. Energy Conf*., 2005, pp. 942–945.

[16] E. Schneiderlöchner, R. Preu, R. Lüdemann, and S.W. Glunz, "Laser-fired rear contacts for crystalline silicon solar cells," *Prog. Photovoltaics, Res. Appl*., vol. 10, pp. 29–34, 2002.

[17] T. Böscke, R. Hellriegel, T. Wütherich, L. Bornschein, A. Helbig, R. Carl, M. Dupke, D. Stichtenoth, T. Aichele, R. Jesswein, T. Roth, C. Schöllhorn, T. Geppert, A. Grohe, J. Lossen, and H.-J. Krokoszinski, "Fully screen-printed PERC cells with laser-fired contacts—An industrial cell concept with 19.5% efficiency," in *Proc. 37th Photovoltaic Spec. Conf*., 2011, pp. 3663–3666.

[18] A. Lorenz, J. John, B. Vermang, E. Cornagliotti, and J. Poortmans, "Comparison of illumination level dependency and rear internal reflectance of PERC-type cells with different dielectric passivation stacks," in *Proc. 26th Eur. Photovoltaic Sol. Energy Conf.*, 2011, pp. 1486–1488.
[19] K.O. Davis, K. Jiang, C. Demberger, H. Zunft, H. Haverkamp, D. Habermann, and W. V. Schoenfeld, "Investigation of the internal back reflectance of rear-side dielectric stacks for c-Si solar cells," *IEEE J. Photovoltaics*, vol. 3, no. 2, pp. 641–648, Apr. 2013.
[20] G. Agostinelli, P. Choulat, H. F. W. Dekkers, E. Vermariën, and G. Beaucarne, "Rear surface passivation for industrial solar cells on thin substrates," in *Proc. 4th IEEE World Conf. Photovoltaic Energy Conv.*, 2006, pp. 1004–1007.
[21] K. Bothe, G.H. Bauer, and T. Unold, "Spatially resolved photoluminescence measurements on Cu(In,Ga)Se_2 thin films," *Thin Solid Films*, vol. 403–404, pp. 453–456, 2002.
[22] W. K. Metzger, I. L. Repins, M. Romero, P. Dippo, M. Contreras, R. Noufi, and D. Levi, "Recombination kinetics and stability in polycrystalline Cu(In,Ga)Se_2 solar cells," *Thin Solid Films*, vol. 517, pp. 2360–2364, 2009.
[23] W.-W. Hsu, J. Y. Chen, T.-H. Cheng, S. C. Lu, W.-S. Ho, Y.-Y. Chen, Y.-J. Chien, and C.W. Liu, "Surface passivation of Cu(In,Ga)Se_2 using atomic layer deposited Al_2O_3," *Appl. Phys. Lett.*, vol. 100, pp. 023508-1–023508-3, 2012.
[24] G. Brown, V. Faifer, A. Pudov, S. Anikeev, E. Bykov, M. Contreras, and J. Wu, "Determination of the minority carrier diffusion length in compositionally graded Cu(In,Ga)Se_2 solar cells using electron beam induced current," *Appl. Phys. Lett.*, vol. 96, pp. 022104-1–022104-3, 2010.
[25] R. Kniese, M. Powalla, and U. Rau, "Evaluation of electron beam induced current profiles of Cu(In,Ga)Se_2 solar cells with different Ga-contents," *Thin Solid Films*, vol. 517, pp. 2357–2359, 2009.
[26] R. Ortega-Borges and D. Lincot, "Mechanism of chemical bath deposition of cadmium sulfide thin films in the ammonia-thiourea system," *J. Electrochem. Soc.*, vol. 140, pp. 3464–3473, 1993.
[27] B. Vermang, V. Fjällström, J. Pettersson, P. Salomé, and M. Edoff, "Development of rear surface passivated Cu(In,Ga)Se_2 thin film solar cells with nano-sized local rear point contacts," *Solar Energy Mater. Solar Cells*, vol. 117, pp. 505–511, 2013.
[28] B. Vermang, *Aluminum Oxide as Negatively Charged Surface Passivation for Industrial Crystalline Silicon Solar Cells*. Leuven, Belgium: Univ. Leuven Press, 2012.
[29] F. Duerinckx, I. Kuzma-Filipek, K. Van Nieuwenhuysen, G. Beaucarne, and J. Poortmans, "Simulation and implementation of a porous silicon reflector for epitaxial silicon solar cells," *Prog. Photovoltaics, Res. Appl.*, vol. 16, pp. 399–407, 2008.
[30] W. N. Shafarman, R. S. Huang, and S.H. Stephens, "Characterization of Cu(InGa)Se_2 solar cells using etched absorber layers," in *Proc. 4th IEEE 4th World Conf. Photovoltaic Energy Conv.*, 2006, pp. 420–423.
[31] J. Lindahl, U. Zimmermann, P. Szaniawski, T. Törndahl, A. Hultqvist, P. Salomé, C. Platzer-Björkman, and M. Edoff, "Inline Cu(In,Ga)Se_2 coevaporation for high-efficiency solar cells and modules," *IEEE J. Photovoltaics*, vol. 3, no. 3, pp. 1100–1105, Jul. 2013. DOI: 10.1109/JPHOTOV.2013.2256232.
[32] P. Salomé, V. Fjällström, A. Hultqvist, and M. Edoff, "Na doping of CIGS solar cells using low sodium-doped Mo layer," *IEEE J. Photovoltaics*, vol. 3, no. 1, pp. 509–513, Jan. 2013.
[33] D. Bae, S. Kwon, J. Oh, W. K. Kim, and H. Park, "Investigation of Al_2O_3 diffusion barrier layer fabricated by atomic layer deposition for flexible Cu(In,Ga)Se_2 solar cells," *Renew. Energ.*, vol. 55, pp. 62–68, 2013.

Bart Vermang received the M.Sc. degree in experimental physics from the University of Ghent, Ghent, Belgium, in 2005, and the Ph.D. degree in electrical engineering from the University of Leuven, Leuven, Belgium, in 2012. During the M.Sc. final research project he studied surface reactions in model metallic catalyst systems at the Norwegian University of Science and Technology (NTNU) in Trondheim, Norway. His Ph.D. research he performed at Imec in Belgium, where he developed novel surface passivation structures for industrial silicon solar cells.

At present, he holds a Postdoctoral position at the University of Uppsala, Uppsala, Sweden, where his challenge is to integrate progressive Si solar cell concepts in CIGS thin-film cells.

Viktor Fjällström was born in Uddevalla, Sweden, in 1986. He received the Master's degree in energy systems engineering from Uppsala University, Uppsala, Sweden, in 2010. The main focus of his studies was renewable energy. His Master thesis was based on experiments in the field of concentrated solar power.

Since the end of 2010, he has been a Research Engineer with the Thin Film Solar Cell Group, Division of Solid State Electronics, Uppsala University.

Xindong Gao received the Ph.D. degree in physics from Fudan University, Shanghai, China, in 2010. His Ph.D. dissertation was based on the study on organic light-emitting device optimization and charge transport mechanisms.

From 2010 to 2011, he held a Postdoctoral. position within the Emerging Electronics group, Division of Solid State Electronics, University of Uppsala, Sweden. The main focus was developing the atomic layer deposition process and the Ni silicide process for advanced complementary metal–oxide semiconductor technology. Since the end of 2011, he has been a Researcher with the same group. His research interests include ion sensors based on both graphene and Si devices with a focus on ion sensitivity and selectivity.

Marika Edoff received the M.Sc. degree in electrical engineering and the Ph.D. degree in solid-state electronics from the Royal Institute of Technology, Stockholm, Sweden, in 1990 and 1997, respectively.

Since 2003, she has been leading research activities on solid-state thin-film solar cells with Uppsala University, Uppsala, Sweden. She was one of the four founders of Solibro, where since 2005, she has also been a part-time employee. Her research interests include CIGS-based thin-film solar cells, with a focus on material synthesis and device characterization.